Article

Journal of Advanced Electrochemical Storage

www.pubj.org

Effect of the templating cationic surfactant assisted with Vanadium Pentoxide on the synthesis and structure of V_2O_5 as tailored Electrode material

F. Regan Maria Sundar Raj[1, *]

[1]Department of Physics, Jeppiaar Engineering College, Chennai 600 119, India.

Cite This: *J. Adv. Electro. Storage* 2025, 1, 21–29

ABSTRACT: A facile synthesis of inimitable hierarchical one-dimensional (1D) V_2O_5 nanorods were successfully developed by simple hydrothermal process. In this work, the effects of the Nature of the Tem-plating Surfactant cetyltrimethylammonium bromide (CTAB) were investigated with atypical concentration in the synthesized samples. The effects of a number of factors, such as the nature of the surfactant, the pH, and the vanadium/ctab ratio in the formation of nanorods V_2O_5 phases were examined by X-ray diffraction, Thermo-gravimetric , differential temperature , Brunauer-Emmett-Teller , Barret-Joyner-Halenda, scanning electron microscope, transmission electron microscope, FT-infrared, FT-Raman and UV–vis reflectance studies exhibit characteristic of ortho-rhombic V_2O_5. It was found that the ordered arrangement crystallinity of the pores was strongly dependent on the vanadium/ctab ratios in the initial batches; too large ratios were unfavorable to the crystallinity. The optimum vanadium/ctab ratio regarding the crystallinity was found to be in the range 1:0.1. The calculated BET specific surface area of V_2O_5-ctab small ratio sample is 10.52 m^2g^{-1}, which is much higher than the surface areas of both V_2O_5-ctab too large (9.37 m^2g^{-1}) and V_2O_5-free (7.5 m^2g^{-1}) samples. High specific surface area and mesoporous nanorods-like morphology of V_2O_5-ctab are the essential factors to show better performance as an electrode material.

1. INTRODUCTION

The apprehension of the dwindling presence of the fossil fuels due to their scarcity in the present electronic era is justifiable and anticipated in modern times. It is likely that the use of the fuels may not last another couple of decades. This is not only because of the depletion of the fuels, but also of the growing use of the energy systems accomplishing the specific aspects such as environment-friendly, non-polluting, renewable aspects of the modern world. This is obvious from the evidence that there is an increasing energy resource crisis, the present crucial challenge the world is facing today. This naturally leads to the need for rechargeable high energy and power density batteries for hybrid motor vehicles and various electronic devices. [1-4] significant studies have been done so far in the direction of analyzing different kinds of batteries and high-performance capacitors. The most hopeful energy storage devices that have been effective in various applications are lithium-ion battery (LIB) and supercapacitors (SCs). The SCs is much better than LIB in both characteristic and application aspects. For instance, the fast charging/discharging ability,

high power density and long cycling stability characteristics are significantly higher that of LIB. The elegant features of SCs favor their potential use in hybrid electrical vehicles, digital communication devices like mobile phones, solar cells and memory back-up devices etc [5]. The distinct nature of SCs is its overall electrochemical performance, which has been improved by the use of innovative electrode materials. To enhance its performance, electrode materials in their cases are to be tailored with high conductivity properties, high porosity to enable easy electrolyte circulation and access of ion to interface for exchange of charges. In this direction, transition metal oxide such as RuO_2, NiO, Co_3O_4, Fe_2O_3, MnO_2, Mo_2O_3, Cr_2O_3, V_2O_5 [6,7]and so forth in low dimension have been intensively investigated as electrode materials owing to the multiple oxidation state. But, among them, vanadium oxide has gained widely attention because of their layered structure, low cost, and extensive oxidation state (V^{2+}, V^{3+}, V^{4+} and V^{5+}) [8]. In most of the research activities related with the nanomaterials, one typical way of experimentation is putting in the right amount of surfactant to obtain changes in the hydrophobic or hydrophilic properties of the mate-rials and thereby modify their surface chemistry. In previous literatures, a wide range of V_2O_5 nanostructures such as nanorods, nanotubes, nanobelts, nanowires, nanoribbons, nanosheets, nanospheres and nanoflowers have been synthesized [7,9]. M. Vadivel et al studied on the influence of various concentration of Cetyltrimethylammonium Bromide (CTAB) cationic surfactant on the properties of $CoFe_2O_4$, the results of which shows enhanced on the dielectric and magnetic properties [10]. In the study conducted by X.L. Xu et al, Flower-like ZnO nanostructure composed of orderly nanoplates synthesized by a CTAB is an excellent promising sensing material for fabricating acetone sensors [11]. Jun bo Zhong et al have prepared TiO_2 with the assistance of CTAB, the results of which demonstrate that the photo catalytic activity of CTAB–TiO_2 is more than three times of TiO2 [12]. Yi Xie et has prepared F—N-codoping TiO_2. This resulted in a new absorption band, which shifted towards higher wavelength on the whole with increasing CTAB concentration [13]. Yan-Xiang Wang et al. reported on ZnO nanopowders by hydrothermal and solvothermal method by using CTAB as surfactant, and the effects of CTAB on the morphologies of ZnO nanopowders were investigated [14]. Devika P. Nair reported CTAB synthesized V_2O_5 displays increasing capacitance compared with V_2O_5 prepared with SDS, PVP and SDBS [15]. However, the lacuna in the past studies is the effect of various concentrations of CTAB in the process of preparation by hydrothermal method. In this present work, we optimize the amount of CTAB concentration tailed with nano-morphological variations and their effects on porosity are meticulously ad-dressed. The use of this tailored Electrode material V_2O_5 will be easier and more environment-friendly and less costly.

2. EXPERIMENTAL

2.1 Material preparation

All reagents were analytical grade and were used without further purification. In a typical synthesis, the proxovanadate was

prepared by dissolving 0.1 mol Ammonium Metavanadate NH_4VO_3 in 80 ml of H_2O and C_2H_5OH solution respectively. Then 0.1 mol of $H_2C_2O_4$ Oxalic acid was added to the solvent to adjust the pH value of the solution ranging from 3h to 4h. After vigorous stirring for 2h until the solution turned to brick-red suspension, it was transferred to a 100 mL of Teflon lined stainless steel autoclave, which was kept in an oven at 120° C for 24 h. The temperature of the autoclave was then cooled down naturally to room temperature and the blue precipitates obtained were collected and washed repeatedly with deionized water and anhydrous ethanol to remove the traces of unreacted residues in the process. Finally, the precipitates were separated by the process of centrifuging and then dried in hot air oven at a temperature of 65° C for 10h. The dried precursor sample was calcined at 400°C for 2h in air. Before calcination the sample is referred as V1 and after calcination the sample is referred as V2. While synthesis using surfactant required amount of surfactant CTAB was added to the precursor solution, after the solution turned to bricked-red suspension and stirred for 1 h. Different concentration of surfactant was studied. V3 referred to surfactant used 10 times lesser quantity to precursor and the surfactant used equal quantity to precursor is mentioned as V4. These nanostructured V_2O_5 samples are investigated in comparison with V2, V3 and V4.

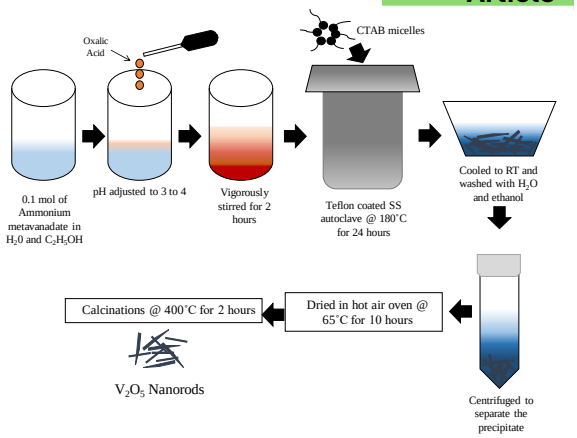

Figure 1. Schematic Illustration of the Synthesis of V_2O_5 by hydrothermal method.

2.2 MATERIALS CHARACTERIZATION

Thermogravimetric analysis (TGA) of the uncalcined precursor samples was carried using Q500V20.10 Build 36 instrument with ramp rate of 20°C per min to determine the water content in the sample from room temperature to 900°C at ambient condition. X-ray diffraction (XRD) analysis was performed using Bruker AXS D8 advanced diffractometer with a high-speed wide angle Lynx Eye Detector for fast collection of data using Cu-Kα (λ = 0.15406 nm). The samples were scanned in the range between 0° and 90° with scan rate of 0.02° per min. Fourier transform infrared (FTIR) spectra were obtained using JASCO FT-IR-4100 spectrometer at room temperature. Raman spectra were measured by using BRUKER RFS 27: Standalone FT-Raman Spectrometer with the laser source of Nd:YAG 1064 nm. Brunauer-Emmett-Teller (BET) Surface Area Analysis and Barrett-Joyner-Halenda (BJH) Pore Size analysis were done by Micromeritics ASAP 2020 analyzer. Surface morphologies of calcined products were examined by High Resolution scanning electron

microscope (HRSEM) using FEI Quanta FEG 200.The chemical composition of the sample was investigated through EDS attached to HRSEM system. High resolution transmission electron micro-scope (HRTEM) images were obtained on JEOL 3010. The DRS UV–vis reflectance spectrum was recorded between 200 nm and 800 nm at room temperature using a PG instrument T90+UV–vis spectrophotometer.

3. RESULTS

3.1 THERMAL ANALYSIS

Thermo-gravimetric analysis (TGA) data and differential temperature analysis (DTA) profiles of the obtained V_2O_5 precursor with various concentration of CTAB are given V2, V3 and V4 in figure 2. From the TGA analysis of the V2, V3 and V4 sample, the first weight loss was observed below 150°C corresponds to the removal of adsorbed water in the precursor. It is associated with one endothermic peak in DTA. Indeed, the endothermic peak is attributed to the removal of water. Whereas the second step at 150°C - 350°C corresponds to the loss of more strongly bond be-tween the layers. It is associated with one endothermic peak below 350°C in DTA attributed to the removal of tightly bound intermolecular water [16]. The TGA plots shows weight of particles sharply decreases up to 7% in V2, 12% in V3 and 43% in V4 associated with DTA plot indexed to combustion and decomposition at 380°C, 400°C and 430°C. The weight loss % increases from V2 to V4 indicates the surfactant assisted synthesized of V_2O_5 precursors. Also, V3 and V4 shows higher weight loss as compared to the surfactant free precursor V2 due to the increase in the mass percentage of CTAB. The endothermic peaks of 680°C suggest the melting point of V_2O_5. As a result above 400°C, it can be assumed that the product completely transforms into the V_2O_5 phase because there is no change in particle weight. In other words, the weight of the sample did not change any more when the temperature went beyond 400°C indicating the stable V_2O_5 was obtained.

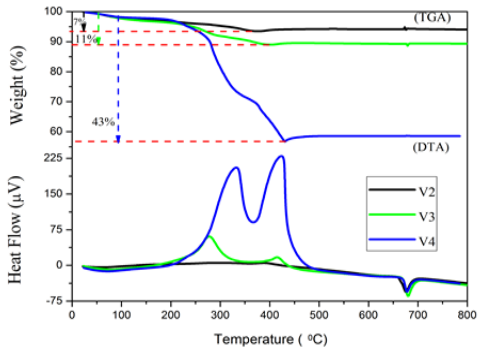

Figure 2. TGA–DTA analysis of as-prepared sample of V2, V3 and V4.

3.2 XRD analysis

X-ray diffraction pattern of the hydrothermally synthesized sample collected with and without various concentration of CTAB added V_2O_5 nanoparticle is shown in figure 3. The as prepared sample (V1) shows poor crystallinity. After annealing the as prepared sample (V1) at 400°C for 2h the collected sample (V2) shows orthorhombic phase V_2O_5. All the diffraction peaks can be indexed to the orthorhombic crystalline phase (space group: C222) of V_2O_5 matched well with the JCPDS Card No. (41-1426) corresponding to the single-shcherbinaite phase with an orthorhombic structure with the lattice parameters a = 11.5086 Å, b = 3.588 Å and c = 4.3670 Å. No other peaks were detected, indicating the high purity of the product. The

diffraction pattern of the V3 and V4 are indexed to the orthorhombic crystalline phase (space group: Pmn21 and P222) of V_2O_5. The calculated lattice parameters for V3 is a = 11.5042 Å, b = 4.3673 Å and c = 3.5599 Å and for V4 is a = 11.4853 Å, b = 4.3648 Å and c = 3.3974 Å. The Scherer's approximation was employed to calculate the average crystalline size for all the samples were in the range of 25-50Å.

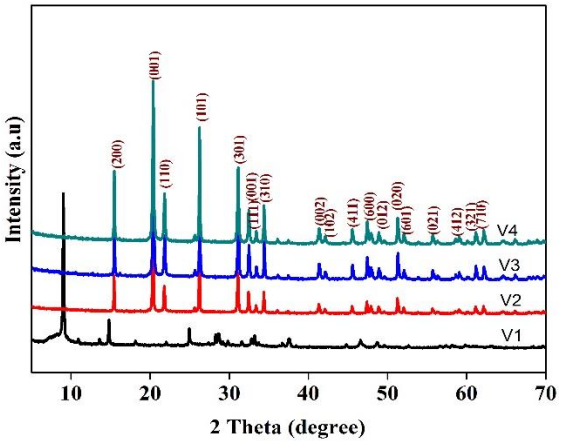

Figure 3. XRD patterns of (V1) samples of as-prepared (V2) synthesized without using surfactant annealed sample at 400°C for 2hrs (V3) synthesized by using CTAB as surfactant (1:0.01), (V4) synthesized by using CTAB as surfactant (1:1).

3.3 SEM–EDS and TEM analysis

The SEM image of V2 shows nanorods morphology with the diameter below 200nm. V3 and V4 with CTAB as a cationic surfactant play a structure directing template in controlling formation of micro and nano architectures. The SEM image of the V3 sample shows nanorods with short diameter range below 100 nm with small aggregates show a drastic change in the diameter of the voids present in the network. Whereas V4 shows nanorods network structure of the material completely collapses and the surface turns into rough surfaces causing several nanorods stack homo epitaxially over one another. It is evident that the weight percentage of CTAB loading on V_2O_5 plays an important role in the morphology of the material. Thus, higher concentration of CTAB collapses the nanorods network with large aggregates. Hence the particles tended to grow together and the gap between the neighboring particles was not easily observed. This suggests the higher percentage CTAB mass loading on V_2O_5 affects the network morphology of the sample. It is also worthy noted that there is sufficient effect of oxalic acid concentration of the structure. It is interesting to find that the addition of various concentrations of CTAB significantly influences the size of the particles. From the HRTEM image, it is clearly observed that the product has high V_2O_5 nanorods structure. SEM images also ensure that all the particles exhibit uniform size and morphology, which is in good agreement with the TEM result. Figure 2 Shows the EDS spectrum of V_2O_5 nanoparticles. No elements other than vanadium and oxygen are detected which confirm the purity of V_2O_5 nanoparticles synthesized in the present work.

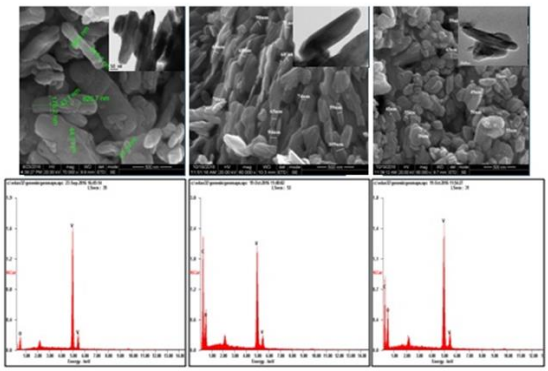

Figure 4. SEM and HRTEM image of the sample V2, V3 and V4 and its corresponding EDX (energy dispersive X-ray analysis) elemental mapping.

3.4 FT-IR Analysis

The structure information of V_2O_5 nanorods is further presented by FTIR spectra as shown in figure 4. These spectra observed in the region from 500 cm^{-1} to 4000 cm^{-1}. In all cases, the spectra exhibited characteristic IR bands corresponding to V_2O_5. The V_2O_5 nanorods exhibit three main vibration modes in the region 600 cm^{-1} to 1020 cm^{-1}. The terminal oxygen symmetric stretching modes (γs) V=O are observed in the range of 825 cm^{-1} to 830 cm^{-1} and 835 cm^{-1}. The bridge oxygen asymmetric and symmetric stretching modes (γas and γs) of V-O-V are observed in 1018 cm^{-1} to 1019 cm^{-1} and 585 cm^{-1} to 630 cm^{-1} [20,21]. IR spectra contain very broad and strong absorption band centered lies in the range of 3437 cm^{-1} to 3456 cm^{-1} are attributed to the presence of stretching and bending modes of the O-H band respectively which affirms the presence of H_2O molecule in synthesized sample, where H_2O is intercalated within the layered structures [22,23].

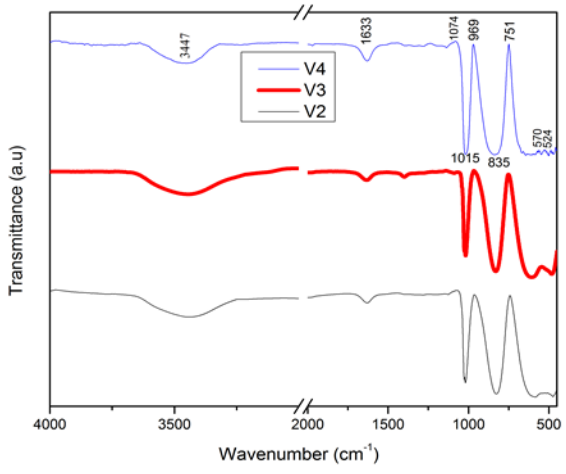

Figure 5. FT-IR spectra of V2, V3 and V4.

3.5 Raman Spectral Analysis

The Raman spectrum of pure V_2O_5 rods reveals that the peaks at 275 cm^{-1}, 401 cm^{-1}, 471 cm^{-1}, 541 cm^{-1}, 686 cm^{-1}, and 989 cm^{-1} are related to the distinct vibrational modes of the orthorhombic V_2O_5 rods. The low frequency modes in the range of 200 cm^{-1} are related to B1g, B3g symmetry and Ag, B2g symmetry attributed to external modes corresponding to the displacement of (VO_5) units with respect to each other. The intensity of these modes thus serves as a good measure of long-range order within the V_2O_5 planes. The higher frequency internal vibrational mode, a sharp Raman band is seen between 987cm^{-1} to 993 cm^{-1} is assigned to the vandyl stretch (V-O_1). The next highest mode at 680 cm^{-1} to 697 cm^{-1} is ascribed to an anti-phase stretching vibration of the (V-O_2). The bending of the V-O3-V bridging unit gives rise to a relative weaker bond at 468 cm^{-1} to 475 cm^{-1} [17-19].

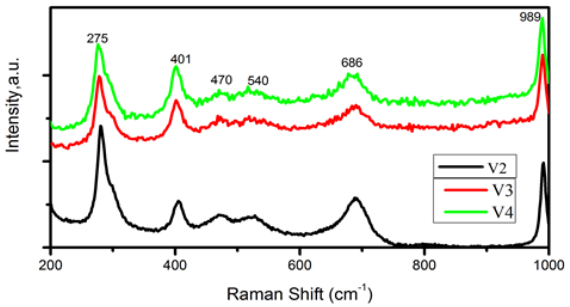

Figure 6. Raman spectra of V2, V3 and V4.

3.6 Optical Band gap energy

The energy band gap of a semiconductor was calculated by the following equation (1)

$$Eg = 1240/\lambda$$

Where Eg is the band gap (eV) and λ is the wavelength (nm) of the absorption edge in

the spectrum. V_2O_5 is a semi- conductor with both direct and indirect energy band gaps, the optical band gap of V_2O_5 for direct and indirect band gap transition was estimated by Tauc equation (2) as follows,

$$(\alpha h\nu)n = K(h\nu - Eg)$$

where α, ν, h, K, and Eg represent the absorption coefficient, photon frequency, Planck's constant, proportionality constant and optical band gap of a semiconductor, respectively; n is dependent on the optical transition type of a semiconductor.

The V_2O_5 sample shows absorption bands in the wavelength range of 200 to 600 nm, based on the reflectance spectrum, the absorption edge was determined. Using the absorption edge values, the bandgap energy was estimated by extrapolating the linear region of the plot. Band-to-band absorption at 400 nm for CTAB surfactant V_2O_5 nanoparticles shows a blueshift in comparison with the pure V_2O_5 which may be ascribed to the quantum confinement effect, due to electronic transitions from occupied 2p bands of oxygen to unoccupied 3d bands of vanadium [25]. Using the absorption edge values, the bandgap energy was estimated by extrapolating the linear region of the plot. The band gaps are about 2.28, 2.29 and 2.27 eV for samples V2, V3 and V4 respectively.

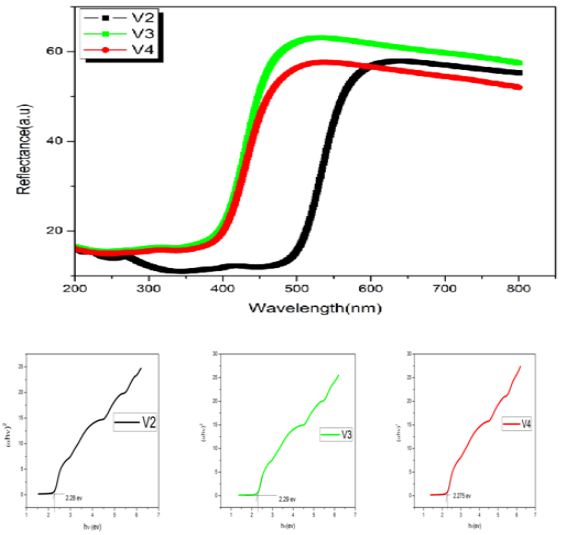

Figure 7. Ultraviolet-visible diffuse reflectance spectra (UV- DRS) of the sample V2, V3and V4.

3.7 Surface Area Analysis

The Barunauer-Emmett-Teller (BET) and porous nature of the sample were investigated by the N_2 Adsorption-desorption method at 77 K. The N_2 Adsorption-desorption isotherm and the corresponding BJH Pore size distribution profile was studied for V2, V3 and V4. The isotherm of all sample indicates a sharp capillary condensation at a high relative pressure and are close to that of a type- IV with H3 type Hysteresis loops according to the International Un-ion of pure and Applied Chemistry (IUPAC) classification owing to its small hysteresis between the adsorption and desorption curves [26]. The hysteresis observed in the pressure P/P0 ranges from 0.45 to 0.99

The BET derived specific surface area of the three samples V2, V3 and V4 are 7.54, 10.52 and 9.37 m^2/g respectively. The highest surface areas among these are V3, followed by V4 and V2 in particular order. The sample V3 to

the precursor: surfactant ratio as 1:0.1, V4 as 1:1 and V2 1:0, it evident that the molar ratio 1:0.1 shows the highest specific surface area with mesoporous network.

Whereas in 1:1 the surface area decreases, suggests the higher concentration of CTAB, this may be the result of some aggregation and rough surface with macroporous as shown in TEM and SEM. Sample V2 shows low surface area without surfactant and the pore structure does not exist .It is evident the surfactant CTAB could etch the surface of the raw V_2O_5 material causing the surface to be porous after annealing. Accordingly, the high surface area and required pore diameter of V2 is expected to provide large number of electrochemical active sites and improve the capacitive behavior during the charge –discharge process.

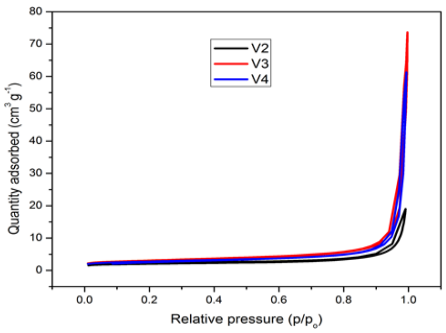

Figure 8. Nitrogen adsorption–desorption isotherms of sample V2, V3 and V4.

4. Conclusion

In summary V_2O_5 nanorods were synthesized with and without surfactant-assisted hydrothermal process. The composition, morphology and structure of the samples were characterized by XRD, RAMAN, IR, UV, BET, SEM and TEM .Surfactant CTAB played a crucial role in the formation of V_2O_5 nanorods. Changing the volume of CTAB will result in a tremendous change of the morphology of V_2O_5. The sample prepared with starting CTAB concentration of 10 times lesser than the precursor quantity showed the BET surface area of 10.52 m^2/g and had more than the surfactant taken equal quantity with the precursor and without surfactant follows as 9.37 m^2/g, 7.5 m^2/g respectively. The present study optimized the concentration of CTAB with V_2O_5 ratio to be 0.1: 1for the formation of uniform nanorods of 50 nm. Our observation possibly will open a new pathway in the development of uniform V_2O_5 nanorods and other structures. Hence the optimization delivers a promising electrode material for supercapacitors.

References

[1] Xu Y, Wang X, An C, Wang Y, Jiao L, and Yuan H A 2014 J. Mater. Chem. 2 16480

[2] Su Q, Huang CK, Wang Y, Fan YC, Lu BA, Lan W et al 2009 J. Alloys and Compd. 475 518

[3] Song C, Gui Y, Xing X, and Zhang W 2016 Mater. Chem. Phy.s 173 460

[4] Li M, Sun G, Yin P, Ruan C, and Ai K 2013 ACS Appl. Mater. Interfaces 5(21) 11462

[5] Bo Wanga, Zhaohui Chena, Gang Lua, Tianhu Wangb and Yunwang Gea 2016 Mater. Res. Bull. 76 37

[6] Saravanakumar B, Purushothaman, KK and Muralidharan, G 2014 Cryst. Eng. 16(46) 10711

[7] Zhang Y, Zheng J, Zhao Y, Hu T, Gao Z, and Meng C 2016 Appl. Surf. Sci. 377 385

[8] Kumar N S, RamanM S, Chandrasekaran J, Priya R, Chavali M, and

Suresh R 2016 Mater. Sci. Semicond. Process. 41 497

[9] Yu W, Wang J, Gou Z, Zeng W, Guo W, and Lin L 2013 Ceram. Int. 39(3) 2639

[10] Vadivel M, Babu R R, Ramamurthi K and Arivanandhan M 2016 Ceram. Int. 42(16) 19320

[11] Xu X L, Chen Y, Ma S Y, Yan, S H, Mao Y Z, Wang T, and Bian H Q 2015 151 5

[12] Li J, Feng F, Huang S, and Zeng J 2013 Mater. Lett. 100 195

[13] Ã Y X, Ã X Z, Li Y, Zhao Q, Zhou X, and Yuan Q 2008 J. Solid State Chem. 181 1936

[14] Wang Y, Sun J, Fan X, and Yu X 2011 37 3431

[15] Nair D P, Sakthivel T, Nivea R, Eshow J S, and Gunasekaran V 2015 15 4392

[16] Du G, Seng K H, Guo Z, Liu J, Li W, Jia et al 2011 RSC Adv. 1690

[17] Foo C Y, Sumboja A, Tan D J H, Wang J and Lee P S 2014 Adv.Energy Mater. 4 1400236

[18] Baddour-Hadjean R, Smirnov M B, Smirnov K S, Kazimirov V Y, Gallardo- Amores J M, Amador U et al 2012 Inorg. Chem. 51 3194

[19] Horrocks G A, Likely M F, Velazquez J M, Banerjee S A 2013 J. Mater. Chem. 1 15265

[20] Li M, Sun G, Yin P, Ruan C, Ai K, 2013 ACS Appl. Mater. Interfaces 5 11462

[21] Yang J, Lan T, Liu J, Song Y, Wei M, 2013 Acta 105 489

[22] Roy A, Pradhan M, Ray C, Sahoo R, Dutta S, Pal T 2014 Cryst.Eng Comm 16 7738

[23] Li H Y, Jiao K, Wang L, Wei C, Lia X, Xie B 2014 J. Mater. Chem. A 2 18806

[24] Chen H, and Xu C, 2016 Materials Letters 166 188

[25] Kumar N S, Raman M S, Chandrasekaran J, Priya R, Chavali M and Suresh R 2016 Mater. Sci. Semicond. Process 41 497

[26] Umeshbabu E and Ranga Rao G 2016 J. Colloid Interface Sci. 472 210